HHS Public Access

Author manuscript

Mol Cancer Res. Author manuscript; available in PMC 2020 June 18.

Published in final edited form as:

Mol Cancer Res. 2019 September ; 17(9): 1828–1841. doi:10.1158/1541-7786.MCR-18-1154.

Identification of Endogenous Adenomatous Polyposis Coli Interaction Partners and β-Catenin-Independent Targets by Proteomics

Olesja Popow[1,2,3], **João A. Paulo**[2], **Michael H. Tatham**[4], **Melanie S. Volk**[3], **Alejandro Rojas-Fernandez**[5], **Nicolas Loyer**[3], **Ian P. Newton**[3], **Jens Januschke**[3], **Kevin M. Haigis**[1,6], **Inke Näthke**[3]

[1]Cancer Research Institute and Department of Medicine, Beth Israel Deaconess Medical Center, Boston, Massachusetts.

[2]Department of Cell Biology, Harvard Medical School, Boston, Massachusetts.

[3]Cell and Developmental Biology, School of Life Sciences, University of Dundee, Dundee, Scotland, United Kingdom.

[4]Centre for Gene Regulation and Expression, School of Life Sciences, University of Dundee, Dundee, Scotland, United Kingdom.

[5]Center for Interdisciplinary Studies on the Nervous System (CISNe) and Institute of Medicine, Universidad Austral de Chile, Valdivia, Chile.

[6]Harvard Digestive Disease Center, Harvard Medical School, Boston, Massachusetts.

Abstract

Adenomatous Polyposis Coli (*APC*) is the most frequently mutated gene in colorectal cancer. APC negatively regulates the Wnt signaling pathway by promoting the degradation of β-catenin, but the extent to which APC exerts Wnt/β-catenin-independent tumor-suppressive activity is unclear. To identify interaction partners and β-catenin-independent targets of endogenous, full-length APC, we applied label-free and multiplexed tandem mass tag-based mass spectrometry. Affinity

Corresponding Author: Inke Näthke, University of Dundee, Dow Street, Dundee, Tayside DD15EH, United Kingdom. Phone: 44-1382-385821; Fax: 44-1382-385386, I.s.nathke@dundee.ac.uk.

Authors' Contributions

Conception and design: O. Popow, J. Januschke, K.M. Haigis, I. Näthke

Development of methodology: O. Popow, A. Rojas-Fernandez

Acquisition of data (provided animals, acquired and managed patients, provided facilities, etc.): O. Popow, J.A. Paulo, M.H. Tatham, M.S. Volk, N. Loyer, I.P. Newton, J. Januschke

Analysis and interpretation of data (e.g., statistical analysis, biostatistics, computational analysis): O. Popow, M.H. Tatham, M.S. Volk, N. Loyer, J. Januschke, K.M. Haigis

Writing, review, and/or revision of the manuscript: O. Popow, J.A. Paulo, M.S. Volk, A. Rojas-Fernandez, N. Loyer, K.M. Haigis, I. Näthke

Study supervision: I. Näthke

Others (generated cell lines, performed screening, sequenced clones, managed mice colonies and carried out westerns): I.P. Newton

The costs of publication of this article were defrayed in part by the payment of page charges. This article must therefore be hereby marked *advertisement* in accordance with 18 U.S.C. Section 1734 solely to indicate this fact.

Disclosure of Potential Conflicts of Interest

No potential conflicts of interest were disclosed.

Note: Supplementary data for this article are available at Molecular Cancer Research Online (http://mcr.aacrjournals.org/).

enrichment-mass spectrometry identified more than 150 previously unidentified APC interaction partners. Moreover, our global proteomic analysis revealed that roughly half of the protein expression changes that occur in response to APC loss are independent of β-catenin. Combining these two analyses, we identified Misshapen-like kinase 1 (MINK1) as a putative substrate of an APC-containing destruction complex. We validated the interaction between endogenous MINK1 and APC and further confirmed the negative, and β-catenin-independent, regulation of MINK1 by APC. Increased Mink1/Msn levels were also observed in mouse intestinal tissue and *Drosophila* follicular cells expressing mutant Apc/APC when compared with wild-type tissue/cells. Collectively, our results highlight the extent and importance of Wnt-independent APC functions in epithelial biology and disease.

Implications—The tumor-suppressive function of APC, the most frequently mutated gene in colorectal cancer, is mainly attributed to its role in β-catenin/Wnt signaling. Our study substantially expands the list of APC interaction partners and reveals that approximately half of the changes in the cellular proteome induced by loss of APC function are mediated by β-catenin-independent mechanisms.

Introduction

Mutations in *Adenomatous Polyposis Coli* (*APC*) are a frequent (>80%) and early event in the development of sporadic colorectal cancer (1, 2). Germline mutations in *APC* also form the genetic basis of familial adenomatous polyposis (FAP), an inherited form of the disease, which is characterized by hundreds of colorectal polyps that progress to cancerous lesions if left untreated (3). This makes a comprehensive understanding of the normal interactions and functions of APC crucial for effectively targeting *APC*-mutant cells.

The tumor-suppressive function of APC has been mainly attributed to its role in Wnt signaling. In conjunction with Axin, APC acts as a scaffold for the β-catenin destruction complex, thereby limiting the transcription of proproliferative β-catenin target genes in the absence of Wnt ligands (4). The vast majority of *APC* mutations result in the translation of a truncated protein and consequent deregulation of Wnt signaling (1, 2). Nevertheless, Wnt-independent roles of APC likely also contribute to its function as a tumor suppressor. This is exemplified by the rare detection of mutations in other Wnt signaling components, including β-catenin, in colorectal cancer (5). Although deletion of *Apc* in the intestinal epithelium in mice phenocopies homozygous truncation mutations, it leads to more rapid onset of tumors despite lower levels of Wnt activation (6). It thus emerges that loss of wild-type (WT) APC confers additional advantages to cells beyond β-catenin-mediated proliferation, but the extent of APC's Wnt-independent functions is unclear.

A variety of proteins have been described to interact with APC in addition to β-catenin destruction complex components (7). However, proteome-wide studies of APC-binding proteins are limited to interactome and yeast-two-hybrid experiments with overexpressed, tagged, and/or fragments of APC (8–11). Using tagged APC in interaction studies is problematic because the C-terminal PDZ-binding domain must remain free to interact with other proteins (12). Similarly, the N-terminal oligomerization domains rely on coiled-coil formation and may be compromised by N-terminal tags (13).To overcome these limitations,

we used label-free affinity-enrichment mass spectrometry (AE-MS) to identify a more comprehensive set of interacting partners of endogenous, nontagged APC. Furthermore, we applied an untargeted global approach using tandem mass tag (TMT)-based and label-free MS to identify proteins that are regulated by APC in their abundance. These two datasets provide a unique resource for the exploration of Wnt/β-catenin-dependent and -independent functions of APC. In addition, we could identify potential targets of APC-containing destruction complexes by combining our data on APC-interacting and APC-regulated proteins (Fig. 1A). Although no direct evidence for the assembly of such complexes by APC exists, other components of the β-catenin destruction complex, such as GSK-3β and $SCF^{\beta\text{-}TrCP}$, are known to have many targets (14, 15). We thus hypothesized that APC may directly regulate the abundance of other proteins in addition to β-catenin.

Materials and Methods

Cell culture

Colo320, HeLa, and SW480 cells were obtained from the ATCC between 2000 and 2010. U2OS cells were obtained from Cell Services at Cancer Research UK in 2006. The HCT116-Haβ92 cell line was a kind gift of Todd Waldman (Georgetown University, School of Medicine, Washington, D.C.), HeLa SEC-C and U2OS SEC-C parental cell lines were a kind gift of Ron Hay (Centre for Gene Regulation and Expression, University of Dundee, Dundee, United Kingdom), the U2OS Flp-In T-Rex host cell line was a kind gift of Carol MacKintosh (Division of Cell and Developmental Biology, University of Dundee, Dundee, United Kingdom). No cell authentication was performed. Cells were grown at 37°C and 5% CO_2 in DMEM with 10% FBS, 50 U/mL penicillin/streptomycin, and 1% v/v nonessential amino acids (all Thermo Fisher Scientific). HeLa SEC-C, U2OS SEC-C, U2OS Flp-In T-Rex, and cell lines generated from these were grown as described above, with the addition of 100 μg/mL hygromycin B and 15 μg/mL blasticidin to the cell culture medium. In all cases, when cells were first received, they were expanded via no more than two passages and then cryopreserved in at least 10–20 aliquots that acted as stocks. Before the use in any experiment, cells were cultured for a minimum of two passages and a maximum of 20 passages after thawing. All cells were routinely tested for *Mycoplasma* contamination every 6 months using MycoAlert (Lonza, catalog no. LT-07–418). Last testing was performed in 2018.

Generation of cell lines

U2OS SEC-C MINK1 knockout cell lines—Analysis of the N-terminal coding region of *MINK1* (ensembl ENSG00000141503) predicted potential gRNAs with high target affinity, high efficiency, and low off-target scores with binding sites in exon 1 and exon 2 using CRISPR Design. We used the best scoring gMINK1 target site in exon 1 (CGGACAGGTCGATGTCGTCC [AGG]) with a score of 95 and 12 predicted off-target sites in other genes. The gRNA sequence was cloned into pBabeD pU6 and sequence-verified. U2OS cells stably expressing Cas9 (U2OS SEC-C) were cotransfected with 3 μg pBabeD pU6 gMINK1 using Lipofectamine 2000 according to the manufacturer's instructions (Thermo Fisher Scientific, catalog no. 11668027). Cells were grown in DMEM supplemented with 10% FBS, 2 mmol/L L-glutamine, and 100 μg/mL normocin (InvivoGen,

catalog no. ant-nr-1). After 12 hours, medium was replaced with fresh medium with 4 μg/mL puromycin. After 48 hours of selection, 2 μg/mL doxycycline was added to induce Cas9 expression. After 72 hours, single cells were sorted with an Influx Cell Sorter (BD Biosciences) into 96-well plates containing DMEM with 20% FBS, 2 mmol/L L-glutamine, 100 U/mL penicillin, 100 μg/mL streptomycin, and 100 μg/mL normocin. MINK1 protein expression was screened by Western blotting analysis. Genomic DNA of MINK1 KO cells was amplified by PCR and sequenced to confirm the introduction of frameshift mutations.

HeLa SEC-C mNeonGreen-MINK1—The same pBabeD pU6 gMINK1 vector used for the generation of MINK1 knockout cells was used for the fusion of mNeonGreen to the N-terminus of MINK1 in HeLa SEC-C cells as described previously (16). A donor vector was designed to replace the ATG start codon of *MINK1* with the start codon of an mNeonGreen cDNA cassette, flanked by approximately 500 bp homology arms. The donor vector was synthesized by GeneArt (Life Technologies). Expression of mNeon-MINK1 in selected and expanded single-cell clones was validated by Western blotting analysis and microscopy.

U2OS Flp-In T-Rex MINK1-GFP/GFP—Stable cell lines with tetracycline/doxycycline-inducible expression of MINK1-GFP/GFP-MINK1 and GFP, respectively, were generated using the Flp-In T-Rex System according to the manufacturer's instructions (Thermo Fisher Scientific) by transfecting U2OS Flp-In T-Rex host cells with pcDNA5 FRT/TO C-GFP, pcDNA5 FRT/TO MINK1-GFP, or pcDNA5 FRT/TO GFP-MINK1, respectively, and pOG44, a constitutive Flp recombinase expression plasmid.

Generation of fly lines and mosaic follicular epithelia

The YFP-fused, endogenously expressed allele $msn^{CPTI003908}$ was recombined with the FRT[82B], *apc1*$^{-}$, *apc2*$^{-}$ chromosome by meiotic recombination. $msn^{CPTI003908}$, FRT[82B], *apc1*$^{-}$, *apc2*$^{-}$ and Hs-*flp*; Ubi-$PH^{PLC\delta1}$::*RFP*; FRT[82B], Ubi-*nls*::*RFP* flies were crossed and *apc1-, apc2*-mutant clones in follicular epithelial cells in the resulting progeny were induced by a 2-hour, 37°C heat-shock at a late (starting to pigment) pupal stage.

Transfections

For siRNA transfections, cells were transfected 1 day after seeding with siGENOME APC siRNA #1-#3 (Dharmacon, catalog no. D-003869–05/06/07), Hs_CTNNB1_5 FlexiTube siRNA (Qiagen, catalog no. SI02662478), or siGENOME Non-Targeting siRNA #1 (Dharmacon, catalog no. D-001210–01-05) using INTERFERin (Polyplus-Transfection, catalog no. 409–10) using 72 ng siRNA/T-25 flask. Colo320 cells were transfected twice on 2 consecutive days. For plasmid transfections, cells were transfected 1 day after seeding with 4 μg myc-tagged β-catenin constructs (17)/10-cm dish using Fugene 6 Transfection Reagent (Promega, catalog no.2691).

Mice

All mice were obtained from The Jackson Laboratory and bred and maintained in accordance with their recommendations under specific pathogen-free conditions in the Biological Resource Unit at the University of Dundee (Scotland, United Kingdom). Compliant with the ARRIVE guidelines, the project was approved by the University Ethical

Review Committee and authorized by a project license (PPL 70/8813) under the UK Home Office Animals (Scientific Procedures) Act 1986.

Protein and RNA harvest

To harvest proteins, cells or cryo-pulverized mouse small intestinal tissue were lysed in 50 mmol/L Tris-HCl pH 7.5, 100 mmol/L NaCl, 5 mmol/LEDTA, 5 mmol/LEGTA, 40 mmol/L β-glycerophosphate, 0.5% NP-40, 1 mmol/L sodium fluoride, 0.1 mmol/L sodium orthovanadate, and 10 μg/mL of each leupeptin, pepstatin A, and chymostatin. Lysates were cleared by centrifugation and supernatants were collected for further processing. mRNA was isolated using the NucleoSpin RNA II Kit (Machery-Nagel, catalog no. 740955.10).

Immunoprecipitations

For APC IPs, 40-μL protein G-sepharose (Sigma-Aldrich, catalog no. P-3296) was washed with protein lysis buffer and incubated for 12 hours with 80 μg (for AE-MS)/20–40 μg (for Western blotting) of ALI-12–28/C-APC 41.1 antibody (both CRUK) or control V5 tag antibody (kind gift of Ron Hay) at 4°C on a rotating wheel. Antibodies were cross-linked to sepharose using bis[sulfosuccinimidyl]suberate (Thermo Fisher Scientific, catalog no. 21580). Antibody-crosslinked sepharose was incubated with pooled cell lysates harvested from 5 15-cm dishes [(AE-MS and validation co-immunoprecipitation (co-IPs)]/10-mg protein lysate (all other APC co-IPs) for 12 hours at 4°C on a rotating wheel.

For GFP IPs, 15-μL GFP-Trap_A Beads (Chromotek, catalog no. gta-100) were washed twice with PBS and twice with protein lysis buffer. Lysates harvested from one 15-cm dish of U2OS Flp-In T-Rex MINK1-GFP/GFP-MINK1/GFP cells grown for 2 days in media containing 75 ng/mL Tetracycline was incubated with the beads for 4 hours at 4°C on a rotating wheel.

Beads were washed repeatedly with 20 mmol/L Tris-HCl ph 7.5, 150 mmol/L NaCl, 1 mmol/L EDTA, 0.05% Triton X-100, and 5% glycerol (for APC IPs), or protein lysis buffer (for GFP-IPs). Proteins were eluted by boiling with 1.3x NuPAGE LDS Sample Buffer (Thermo Fisher Scientific, catalog no. NP0008).

SDS-PAGE and Western blotting

Protein samples [50 μg (cell lysates) or 100 μg (tissue lysates)] were separated on precast NuPAGE 4%−12% gradient Bis-Tris polyacrylamide protein gels (Thermo Fisher Scientific, catalog no. NP0322/NP0321), transferred to nitrocellulose membrane, and blotted with primary antibodies: anti-ABI2 (catalog no. 302–499A, RRID: AB_1966095), anti-GIT1 (catalog no. 302–101A, RRID: AB_1604200), anti-GIT2 (catalog no. 302–103, RRID: AB_1604269), anti-RNF20 (catalog no. 300–714A, RRID: AB_533428), anti-hPrp3p (catalog no. 302–073A, RRID: AB_1604202), anti-MINK1 (catalog no. A302–192A, RRID: AB_1659822), anti-PAK1 (catalog no. 301–259A, RRID: AB_890620), anti-PDZ-GEF2 (catalog no. 301–967A, RRID: AB_1548003), anti-RNF25 (catalog no. 303–844A, RRID: AB_2620195; all Bethyl Laboratories); anti-Aurora B (catalog no. ab2254, RRID: AB_302923), anti-CASK (catalog no. ab99039, RRID: AB_10696957), anti-LATS1 (catalog no. ab70562, RRID: AB_2133360; all Abcam); anti-GAPDH (Millipore, catalog

no. MAB374, RRID: AB_2107445); anti-GFP (Clontech Laboratories, catalog no. 632381; RRID: AB_2313808); anti-LSM7 (catalog no. 18941–1-AP, RRID: AB_10596483), anti-TBP (catalog no.66166–1-Ig, both Proteintech) anti-β-catenin (BD Transduction Laboratories, catalog no. 610154, RRID: AB_397555); sheep polyclonal anti-GFP (MRC PPU Dundee, S268B); mouse monoclonal anti-APC N-terminus (CRUK, ALI-12–28); rabbit polyclonal anti-APC N-terminus (18); anti-β-catenin (19). Anti-mouse/rabbit Alexa Fluor Plus 800/680-conjugated secondary antibodies (Thermo Fisher Scientific, catalog no. A32735, RRID: AB_2633284/catalog no. A32730, RRID: AB_2633279/catalog no. A32734; RRID: AB_2633283/catalog no. A32729, RRID: AB_2633278) were detected and quantified with the Li-Cor Odyssey imaging system and Image Studio Software.

Immunofluorescence and live imaging

Cells—For immunofluorescence, cells grown on collagen-coated No. 1.5 cover glass were fixed for 10 minutes with −20 °C methanol, permeabilized using 1% NP40 in PBS for 10 minutes, and incubated with IF blocking buffer (5% normal goat serum, 2% w/v BSA, 0.1% Triton X-100 in 1 × PBS) for 30 minutes at room temperature. Cells were washed with 0.2% w/v BSA in 1 × PBS, in between steps. Anti-MINK1 antibody (Thermo Fisher Scientific, catalog no. PA5–28901, RRID: AB_2546377) was diluted 1:250 in blocking buffer without serum and incubated overnight at 4°C. After repeated washing, cells were incubated for 1 hour with 20 μg/mL Hoechst 33342 (Invitrogen, catalog no. H3570) and Alexa Fluor 594 anti-rabbit antibody (Thermo Fisher Scientific, catalog no. PA5–28901; RRID: AB_2546377) diluted 1:500. Cover slips were mounted onto microscopy slides using 90% glycerol with 0.5% N-propyl gallate. For live imaging, cells were grown on 35-mm glass bottom dishes (ibidi, catalog no. 81418–200) in DMEM without phenol red. Images were acquired with an inverted Nikon Eclipse Ti-E fluorescence microscope equipped with a Hamamatsu ORCA-R^2 digital CCD camera and a Prior Scientific Lumen 200PRO light source, using a Plan Apo 60x NA 1.4 objective lens. Images were acquired with the Meta-Morph software (version 7.8.12.0) and without camera binning. 395/25; 480/40; and 545/30 excitation and 460/50; 535/50; and 620/60 emission filters were used for Hoechst, mNeonGreen, and Alexa594. Image brightness and contrast was adjusted equally for each image using Fiji software (20).

Drosophila egg chambers—Msn::YFP-expressing, mosaic *apc1*$^{-}$, *apc2*$^{-}$-mutant female flies were dissected 24 hours after hatching. Ovaries were dissected into individual ovarioles in glucose- (1 g/L) and insulin- (0.2 g/L) supplemented Schneider's medium (Lonza, catalog no. Iz04–351q) in a 35-mm glass bottom dish. Imaging was performed on a SP8 Confocal Microscope (LEICA) equipped with a 63x NA 1.2 water immersion objective within the hour following dissection. The Nls::RFP marker was used to discriminate *apc1*$^{-}$, *apc2*$^{-}$-mutant cells, *apc1*$^{+}$, *apc2*$^{+}$ control cells and *apc1*$^{-}$, *apc2*$^{-}$/*apc1*$^{+}$, *apc2*$^{+}$ heterozygous control cells. Msn:: YFP levels were measured at the interface between cells of the same genotype and, for each egg chamber, normalized to the median value measured at the interfaces between heterozygous control cells.

Cell adhesion assay

Ninety-six-well plates coated with 10 μg/cm^2 collagen (Sigma-Aldrich, catalog no. 8919) were washed with PBS and incubated for 1 hour with DMEM + 0.5% BSA at 37°C. Cells were detached with 10 mmol/L EDTA in PBS for 10 minutes at 37°C, washed twice with DMEM, counted using a Cellometer Auto T4 Bright Field Cell Counter (Nexcelom Bioscience), and diluted to a density of 1 × 10^5 cells/mL in DMEM + 0.1% BSA. A total of 10,000 cells were added per well and incubated for 1 hour at 37°C. Loosely attached cells were removed by vigorous shaking of the plate for 10 seconds, and washing with DMEM + 0.1% BSA. Adherent cells were fixed with 4% paraformaldehyde for 10 minutes, washed, and stained for 10 minutes with 5 mg/mL crystal violet in 2% ethanol. Plates were washed once with water and then dried overnight. Crystal violet stain was solubilized with 200 μL 2% SDS/well for 30 minutes and diluted 1:4 with water. Absorption was measured at 550 nm using a Synergy H1 Hybrid Multi-Mode Microplate Reader (BioTek).

MTT cell proliferation assay

Cells were seeded 1 day after transfection into 96-well plates with 1 × 10^5 cells/well. Viable cells were measured using the TACS MTT Proliferation Assay Kit (Trevigen, catalog no. 4890–25-01 and catalog no. 4890–25-02).

qRT-PCR

cDNA was synthesized using the qScript cDNA Synthesis Kit (Quanta Biosciences, catalog no. 95047). qRT-PCR reactions were performed in triplicate using PerfeCTa SYBR Green FastMix (Quanta Biosciences, catalog no. 95072) and a CFX Connect Real-Time PCR Detection System (Bio-Rad). C_T values obtained for target genes were normalized to *ACTB* and relative mRNA expression was calculated using the Pfaffl method (21). Primer sequences: *ACTB* forward/reverse-CTGGGAGTGGGTGGAGGC/TCAACTGGTCTCAAGTCAGTG, *AXIN2* forward/reverse: TGGCTATGTCTTTGCACCAG/TGTTTCTTACTGCCCACACG, *CTNNB1* forward/reverse: ATGGCTTGGAATGAGACTGC/TTCCATCATGGGGTCCATAC, *MINK1* forward/reverse: TCAACCTGCTCATCACCATC/TCCACTTCTGGGTCATTGTG.

Protein analysis by mass spectrometry

For label-free MS analysis, co-IP and complete lysate samples were separated by SDS-PAGE and proteins were visualized by Coomassie Blue staining. Gel lanes were subdivided into three parts: gel regions containing coeluted antibody heavy and light chains in co-IP samples were pooled. In-gel tryptic digestion was performed as described previously (22). Peptides solubilized in 1% FA were analyzed by LC-MS/MS on a Q Exactive Mass Spectrometer (Thermo Fisher Scientific) coupled to an EASY-nLC 1000 liquid chromatography system via an EASY-Spray Ion Source (Thermo Fisher Scientific) with a 75 μm × 500 mm EASY-Spray Column (Thermo Fisher Scientific) heated to 40°C. An elution gradient duration of 240 minutes was used, fractionating mostly over the 3%−40% acetonitrile range. Data were acquired in the data-dependent acquisition mode. Full-scan spectra (300–1,800 Th) were acquired with resolution of 70,000 at 400 Th (after accumulation to a target value of 1,000,000 with maximum injection time of 20 ms). The ten

most intense ions were fragmented by higher-energy collisional dissociation and measured with resolution 17,500 at 200 m/z and a target value of 500,000, with a maximum injection time of 60 ms. Intensity threshold was $2.1e^4$. Unassigned, +1, and >8+ charge peptides were excluded, and peptide matching was set to "preferred." A 40-second dynamic exclusion list was applied.

For TMT-label MS analysis samples were processed as described previously (23).

Two micrograms of each sample were analyzed on an Orbitrap Fusion Lumos mass spectrometer coupled to a Proxeon EASY-nLC 1200 liquid chromatography pump (both Thermo Fisher Scientific) and a 100 μm × 35 cm microcapillary column packed with Accucore C18 Resin (2.6 μm, 150 Å; Thermo Fisher Scientific). Peptides were fractionated over a 150-minute gradient of 3%−25% acetronitrile in 0.125% formic acid. An MS^3-based TMT method was used, as described previously (24).

Raw MS data analysis

Raw MS data files were processed using MaxQuant (25, version 1.5.8.3) using default settings. MS/MS spectra were searched against the UniProt human proteome sequence database. The MaxLFQ algorithm was implemented, applying a minimum ratio count of 2. For label-free samples the "match between runs" option with default settings was enabled. TMT-labeled samples were quantified by reporter ion MS^3 - TMT10plex (Lys & N-terminal 126C-130N), with a reporter mass tolerance of 0.003 Da. One percent FDR filtering was applied at protein and peptide levels.

MS data processing

Further MS data analysis was performed using Perseus (26, version 1.5.8.5). "Reverse" proteins, proteins "only identified by site," and all nonhuman contaminants and human contaminants, except cytoskeletal components, were filtered out. Data were $\log_2$-transformed. The filtered APC AE-MS dataset contained 5,571 identified proteins, of which 5,521 were measured. From these, only proteins measured in all four replicates of at least one IP with N-APC, C-APC, or control antibody were carried forward (4,016 proteins). Missing values were imputed from a normal distribution using standard settings (width: 0.3 × SD of measured values, down shift: 1.8 in units of Sd of measured values).

The filtered label-free proteome dataset contained 5,982 identified proteins, of which 4,927 were measured in at least three replicates of at least one condition and only these were used for further analysis. Missing values were imputed from a normal distribution.

The filtered TMT proteome dataset contained 6,949 identified proteins, of which 6,923 were measured in all analyzed samples. Only these proteins were used for further analysis.

Enrichment analysis of category terms within the group of potential APC interactors identified by AE-MS (171 proteins) relative to all proteins measured in this experiment (4,016 proteins) was calculated by Fisher exact test using default settings with a Benjamini-Hochberg FDR < 0.02 used for truncation.

Network generation

The APC interaction network was generated in Cytoscape (27, version 3.5.0) using information on APC interactors listed in the IntAct Molecular Interaction Database and/or BioGRID interaction repository. Low-confidence links (IntAct MI score < 0.6), individual nodes detached from the network, and indirect APC interactors with less than two connections were deleted. The network layout was generated using the Weak Clustering algorithm and the IntAct MI score for edge weighting within the Cytoscape Allegro Layout App.

Results

Identification of APC-interacting proteins by AE-MS

For our initial discovery experiments, we used HeLa cells, which express relatively high amounts of WT APC that can be efficiently depleted by siRNA. This allowed us to measure protein binding to, and regulation by, APC in the same cell line. APC-containing protein complexes were coimmunoprecipitated using two APC-specific mAbs that recognize N- and C-terminal domains, respectively. An isotype-matched antibody against the viral V5 peptide was used as control. co-IP with each antibody was performed in quadruplicate. Samples were analyzed by label-free LC/MS-MS. We only considered the 4,016 proteins that were detected in all four replicates of co-IP's with either antibody for further analysis. Pearson correlation coefficients >0.9 for label-free quantification (LFQ) intensities measured across replicates and a clear separation of N-APC, C-APC, and control co-IPs by principal component analysis (PCA) indicated good experimental reproducibility (Supplementary Fig. S1A and S1B). Significant enrichment of proteins in APC-specific versus control co-IPs was determined by considering both permutation-based FDR (<0.01) and LFQ intensity fold change (Supplementary Fig. S1C).

In total, 171 proteins were significantly enriched in APC-specific co-IPs (Fig. 1B; Supplementary Table S1). These proteins will be referred to, hereafter, as the "APC interactome." Eighty and 71 proteins were exclusively enriched in either C-APC or N-APC co-IPs, respectively. Antibody binding to APC is likely affected by protein interactions at domains close to or overlapping with the antibody epitopes. This could explain coimmunoprecipitation of distinct interactors with different APC-specific antibodies. Consistently, C-APC and N-APC antibodies immunoprecipitated overlapping, but distinct, pools of APC that may contain different subsets of binding partners (Supplementary Fig. S1D). Twenty proteins, including APC itself, were significantly enriched in both APC co-IPs and only half of these were previously described APC interactors (28, 29; Supplementary Table S1).

To rule out a HeLa cell-specific enrichment of proteins in APC co-IPs, we validated our AE-MS results in the human colon carcinoma cell line HCT116-Haβ92, which are homozygous for WT APC and hemizygous for WT β-catenin (30). Thirteen of the novel APC-interacting proteins were selected to cover the range of biological functions represented in the dataset and based on antibody availability. Consistent with results obtained by AE-MS, 12 of 13 proteins were enriched in APC co-IPs in both cell lines (Supplementary Fig. S2).

The APC interactome is enriched for epithelial-specific gene ontology cellular component terms

To identify underlying functional patterns, we analyzed the enrichment of gene ontology (GO), protein family (Pfam), and Kyoto encyclopedia of genes and genomes (KEGG) terms in the APC interactome. Thirty-one terms were significantly overrepresented (Benjamini-Hochberg FDR < 0.02); the majority can be broadly categorized into three cellular processes: (actin) cytoskeleton organization, cell-cell contact establishment, and RNA processing (Fig. 1C; Supplementary Table S1). APC-interacting proteins associated with cytoskeletal organization included known and newly identified interactors, including several SCAR complex components. The enrichment of terms linked to RNA processing is consistent with APC's role as an RNA-binding protein (31). Strikingly, many of the enriched terms are associated with cell-cell contacts and constitute components characteristic of epithelial cells, for example, "lateral plasma membrane," "tight junctions," and "cell-cell adherens junction."

Generation of an integrated APC interaction network

To understand the relationship between interaction partners, we tested how our interactome integrated into a network of previously identified APC-binding proteins. Our interactome dataset overlaid well with, and added substantially to, the network of known APC-binding proteins (Fig. 2). The integrated network revealed many direct and indirect high-confidence links between newly identified and known APC interactors suggesting potential APC-interacting protein complexes. In addition to the "β-catenin destruction complex" cluster, several subnetworks emerged from this analysis. Two of these included proteins associated with "LSM protein family" and "SCAR complex," respectively, and both categories were enriched in our APC interactome dataset (Fig. 1C).

To validate our network analysis, we generated a control network using 171 proteins randomly selected from the APC AE-MS dataset. Compared with the random selection, our interactome exhibited superior integration into the network of known APC-binding partners (Supplementary Fig. S3).

APC affects the abundance of many proteins independently of β-catenin

Because our APC interactome included many binding partners that appeared unrelated to Wnt signaling components, we aimed to determine whether APC is involved in the regulation of proteins other than β-catenin, and independently of β-catenin-mediated cellular effects. To this end, we depleted APC alone or together with β-catenin from HeLa cells using siRNA and measured changes in protein abundance by mass spectrometry (MS). Cells were harvested 72 hours after transfection and efficient knockdown was confirmed by Western blotting (WB, Supplementary Fig. S4A). Simultaneous knockdown of APC and β-catenin abrogated β-catenin target gene activation, as verified by the inhibition of *AXIN2* mRNA transcription (Supplementary Fig. S4D). For each siRNA combination, we analyzed four and two experimental replicates by label-free and TMT MS, respectively. Downstream analysis was applied to 6,923 proteins measured in all eight samples by TMT MS and 4,927 proteins measured in at least three replicates of at least one condition by label-free MS. Reproducibility between replicates was very good, as indicated by Pearson correlation

coefficients >0.97 and a clear separation of distinct siRNA treatments by PCA (Supplementary Fig. S4B and S4C).

To identify proteins that changed in abundance in response to APC depletion, but independently of β-catenin, we compared TMT/LFQ intensities across conditions of all measured proteins to an “ideal” intensity profile of a hypothetical β-catenin-independent APC target. A negative APC target was defined as a protein that increased in abundance in response to APC loss, independently of whether APC was depleted alone or together with β-catenin, but which protein levels did not change in β-catenin siRNA compared with control siRNA-treated cells (the intensity profile of an “ideal” negative APC target is indicated in red in Fig. 3A top right). Conversely, a positive APC target was defined as a protein that decreased in abundance in response to APC depletion, independent of β-catenin status. The 200 proteins with profiles most similar to the ideal negative and positive APC target were selected on the basis of Pearson correlation. Significant β-catenin-independent APC targets were determined by applying an additional cutoff of >1.5 fold change in APC and APC+β-catenin siRNA-treated samples relative to control with a *q*-value <0.05 (TMT)/0.1 (LFQ). By TMT MS we identified 53 and 85 proteins that significantly increased and decreased, respectively, in response to APC depletion in a β-catenin-independent manner; by LFQ MS 11 proteins increased and 11 decreased (Fig. 3A/B and E/G). Four negatively and seven positively regulated proteins were common to both datasets. This group of proteins was not enriched in distinct GO terms (data not shown), but spanned a range of cellular functions including apoptosis, ion transport, actin organization, and proliferation.

To compare APC’s β-catenin-dependent and -independent effects on protein expression, we also identified proteins that changed in abundance in response to APC depletion in a β-catenin-dependent manner. The number of these proteins was similar to those regulated independently of β-catenin: 64 and 37 were negatively regulated, 86 and 103 were positively regulated when detected by TMT and LFQ MS, respectively (Fig. 3C/D and F/H; Supplementary Table S2).

Some β-catenin-independent APC targets are also deregulated in human cancer

To determine whether any of the identified β-catenin-independent APC targets are implicated in colorectal cancer, we compared our results with a dataset describing proteomic changes in human colorectal adenoma and adenocarcinoma compared with healthy mucosa (32). Nineteen proteins present in our APC target list were also found to be dysregulated, in the same direction, in human adenomas and/or carcinomas (Table 1). These results highlight that misexpression of some proteins in colorectal cancer could be a direct consequence of loss of WT APC rather than deregulated Wnt signaling.

MINK1 interacts with full-length and truncated APC

From the group of β-catenin-independent APC targets identified by total proteomics analysis, six were also found to interact with APC. Amongst these, MINK1 stood out as a potentially druggable serine/threonine kinase. We validated the interaction between MINK1 and full-length APC by co-IP and WB in two cell lines (Fig. 4A). In agreement with results obtained by MS, MINK1 was only enriched in co-IPs with the N-APC antibody

(Supplementary Fig. S5A). To rule out N-APC antibody cross-reactivity, we repeated the experiment with lysate from APC-depleted cells. Confirming its specific enrichment in APC protein complexes, the amount of coimmunoprecipitated MINK1 correlated with the levels of APC present in IP lysates (Supplementary Fig. S5B). Conversely, APC was also enriched in co-IPs of overexpressed GFP-tagged MINK1 compared with GFP alone (Supplementary Fig. S5C). We next tested whether MINK1 could also interact with truncated APC expressed in colorectal cancer cells. MINK1 coimmunoprecipitated with APC fragments in both SW480 and Colo320 cells (Fig. 4B). The approximately 90 kDa N-terminal APC fragment expressed in Colo320 cells retains the armadillo and oligomerization domain, but lacks all β-catenin and Axin-binding sites and other C-terminal domains. The approximately 220 kDa APC fragment expressed in SW480 cells includes the four most N-terminal β-catenin-binding sites. These data suggest that the interaction between the two proteins is mediated by domains in the N-terminal third of APC.

MINK1 is negatively regulated by APC independently of β-catenin

Consistent with our proteomics data, MINK1 levels measured by WB significantly increased after 72 hours of APC depletion in HeLa and U2OS cells and this accumulation was independent of changes in β-catenin (Fig. 4C; Supplementary Figs. S5D and S6A). Similar to results obtained with the siRNA pool, transfection with either of the individual APC siRNAs efficiently decreased APC levels and produced a concomitant increase in MINK1 protein (Supplementary Fig. S5E). We validated the effect of APC loss on MINK1 levels *in vivo* by measuring protein expression in intestinal tissue from *Apc*-mutant and WT mice. MINK1 protein was increased by 2.3-fold (±0.4 SD) in $Apc^{Min/+}$ versus control animals (Fig. 5A and B). In addition, we addressed whether this regulatory relationship is conserved across species. We generated mosaic follicular epithelia in *Drosophila melanogaster* egg chambers carrying clones of double *APC1, APC2*-mutant cells (marked by loss of NLS::RFP expression). Measuring levels of a YFP-fused Misshapen protein, the closest orthologue in *Drosophila,* (Msn::YFP) using live microscopy revealed that Msn::YFP levels were significantly higher in cells that did not express APC1 and APC2 (Fig. 5C–F).

Parallels between the regulation of MINK1 and β-catenin protein abundance

We hypothesized that APC regulates the abundance of MINK1, similarly to β-catenin, posttranscriptionally. Transfection with APC siRNA resulted in a significant upregulation of *AXIN2* mRNA, and this increase was efficiently inhibited when APC and β-catenin were depleted simultaneously. In contrast, *MINK1* mRNA increased moderately but changes in *MINK1* mRNA did not correlate with changes in MINK1 protein abundance (Fig. 6A and C).

We further tested whether the degradation of MINK1, similarly to β-catenin, was dependent on the action of an E3 ubiquitin ligase. Treatment with the NEDD8-activating enzyme selective inhibitor MLN4924, which inhibits cullin-RING ubiquitin ligase activity (33), reproducibly induced a 2-fold increase in MINK1 after 24 hours (Fig. 6B; Supplementary Fig. S6B).

MINK1 localizes to cell-cell junctions and enhances cell adhesion and proliferation

To address how elevated MINK1 could contribute to cellular processes affected by *APC* mutations, we determined its subcellular localization. In agreement with a previous study (34), immunofluorescence staining showed an enrichment of signal in the perinuclear region (Supplementary Fig. S6C). Nevertheless, a similar signal was present in MINK1 knockout cells, suggesting cross-reactivity of this MINK1 antibody with Golgi components. Indeed, the MINK1 antibody used for immunofluorescence recognized additional proteins by WB (Supplementary Fig. S6D; the MINK1 antibody we used for WB was unsuitable for immunofluorescence).

To overcome this problem, we generated cells expressing endogenously mNeonGreen-tagged MINK1 (Supplementary Fig. S6D), enabling us to study its localization live in unfixed cells (Fig. 6C). Although fluorescence intensity was low, mNeonGreen signal was clearly enriched at tips of protrusions (*) and at lateral plasma membranes (arrow heads) in areas of cell-cell contact (Fig. 6C). No signal enrichment was detected in “free” regions of the plasma membrane without adjoining cells. Consistent with a role for MINK1 in adhesion, overexpression of MINK1 resulted in a significant increase in cell attachment to collagen (Fig. 6D; Supplementary Fig. S6E). Furthermore, proliferation of colorectal cancer cells, in which regulation of MINK1 by APC was lost (Supplementary Fig. S6F), was significantly reduced when MINK1 was depleted using siRNA (Fig. 6E).

Discussion

We aimed to elucidate, on a global scale, the diverse molecular roles of APC, with an emphasis on its functions beyond the β-catenin destruction complex. To this end, we applied an untargeted approach using label-free and TMT-based MS to assemble an APC interactome and, furthermore, to identify the β-catenin-independent APC-regulated proteome. These datasets provide a useful resource for the identification of proteins that participate in and coordinate Wnt-independent functions of APC.

In contrast to previous interaction studies, we used endogenous, full-length, and nontagged APC in our AE-MS experiment. The identification of additional PDZ domain-containing APC interaction partners highlighted the benefit of this approach.

Strikingly, the APC interactome was highly enriched for proteins that are part of cellular components characteristic for epithelial cells, as well as members of the membrane associated “guanylate kinase” (MAGUK) protein family, and PDZ domain-containing proteins (Fig. 1C). MAGUK proteins are implicated in the establishment of epithelial cell polarity (35). Furthermore, the function of APC in epithelia is, at least partly, mediated by PDZ domain-containing proteins (36). In addition, STRIPAK complex components formed a highly connected cluster within the APC interaction network (Fig. 2). APC and the STRIPAK component Striatin localize interdependently to cell-cell junctions in epithelial cells and depletion of Striatin and APC affects tight junction organization (8). It is conceivable that binding to APC regulates the subcellular localization, activity, and/or expression of these epithelial-characteristic proteins, in turn controlling cellular adhesion and establishment of epithelial polarity. Investigating these interactions further will provide

useful insights into the mechanisms that regulate APC function in different tissues and further improve our understanding of the phenotypes associated with APC loss. Such studies could reveal why *APC* germ line mutations in patients with FAP result in cancerous lesions of the gut epithelium, while other organs often remain unaffected.

Measuring proteome-wide effects of APC loss revealed a set of β-catenin-independent APC targets, supporting a role of APC in the regulation of protein abundance beyond the β-catenin destruction complex (Fig. 3). Similar to the effect on β-catenin, depletion of APC resulted in the accumulation of some proteins, while the levels of others were negatively affected, suggesting that APC can also inhibit degradation of some of its targets. Strikingly, the number of proteins regulated by APC independent and dependent of β-catenin was very similar. It is important to acknowledge that untargeted MS is biased toward detection of more abundant proteins. Consistently, many established, but low-abundant, β-catenin targets, such as Myc and Axin2, were not detected and are thus absent from our analysis. However, this bias operates in both sets of targets equally. Changes in the abundance of individual APC targets could result from alterations in PTMs and/or protein stability—as is the case for β-catenin. This is supported by previous findings in *Drosophila,* where loss of APC2 causes proteome-wide and β-catenin-independent changes in posttranslational modifications that also affect protein stability of some proteins (37). In addition, effects on transcription may also contribute to the differences in protein abundance observed in our study.

Because we have used HeLa cells (which we chose for technical reasons, see Results section) in our discovery MS experiments, we were unable to identify potential APC-interacting proteins and/or targets whose expression is, for example, restricted to intestinal epithelial cells. This limitation will need to be addressed in future studies—ideally using human/mouse intestinal tissue expressing WT and mutant APC.

At present, it remains unclear how changes in these APC targets contribute to the functional consequences of APC loss observed *in vivo.* As a first step toward addressing this question, we compared our dataset with data describing proteome-wide changes in colon adenomas and carcinomas (32). Several of the β-catenin-independent APC targets we identified were also found to be dysregulated in colorectal adenomas and/or tumors (Table 1). Among these, NDRG1, which was downregulated in APC-depleted cells in our study and also in cancerous tissue, might be of particular interest. NDRG1 has been established as a tumor suppressor in colorectal cancer cells based on its negative effects on metastasis and apoptosis (38).

Collectively, our results suggest that part of the protein expression changes observed in colorectal cancer are independent of increased Wnt target gene expression. Investigating the functional impact of these changes will further help to elucidate how APC loss contributes to cancer development beyond deregulated β-catenin. Accounting for these effects will be especially important when considering cancer therapy, as they reveal that consequences of mutant APC protein cannot be fully rectified by restoring normal Wnt signaling.

Little is known about the functions of MINK1 or the regulation of its activity and/or its abundance. Existing data implicate MINK1 in cell adhesion, cell migration, and planar cell polarity (PCP; 34, 39, 40)—processes crucial for epithelial biology. Furthermore, MINK1

kinase activity is required for completion of cytokinesis (41). Importantly, these processes are also deregulated in APC-mutant tissues (42–44). Moreover, TRAF2 and NCK-interacting protein kinase, which shares high sequence homology with MINK1, is emerging as a promising target for colorectal cancer therapy, as it regulates the activity of the TCF-4/β-catenin transcription complex (45).

Collectively, our results indicate that MINK1 is regulated by APC in a manner similar to β-catenin (Figs. 4 and 6). Importantly, increased MINK1/Msn levels after loss of WT APC/APC1,2 were also observed *in vivo,* in mouse intestinal tissue and follicular cells in *Drosophila* (Fig. 5). Consistent with its localization to cell-cell junctions, overexpression of MINK1-GFP resulted in increased cell adhesion (Fig. 6C and D). This is in contrast to a previous study, in which cells overexpressing full-length MINK1 did not grow in clusters but in isolation, suggesting decreased adhesion between cells (34). However, in this case, the effects were not quantified and additional studies of MINK1 overexpression on cell-cell adhesion do not exist. It is conceivable, that enhanced cell adhesion due to elevated MINK1 expression contributes to the reduced cell migration observed in *APC*-mutant tissue (43, 46). Moreover, directionality of cell migration could be disturbed when MINK1 expression is deregulated in response to APC loss. Evidence for a role of mammalian MINK1 in PCP is limited (39); however, a role for its *Drosophila* homologue Msn in epithelial PCP has been firmly established (47). In flies, both APC and Msn act downstream of Dishevelled, which was described as a “branchpoint” between the canonical Wnt and the noncanonical PCP pathway (48). Our results indicate that regulation of Msn by APC is conserved in flies (Fig. 5C–F), suggesting an additional level of cross-talk between these signaling pathways. Furthermore, knockdown of MINK1 in colorectal cancer cells resulted in a significant reduction in proliferation, comparable with the effect seen with β-catenin depletion (Fig. 6E). Future experiments will focus on elucidating the molecular mechanisms of MINK1 regulation by APC and the identification of downstream effectors mediating the effects of MINK1 overexpression on cell adhesion.

Supplementary Material

Refer to Web version on PubMed Central for supplementary material.

Acknowledgments

We are grateful for the following financial support: O. Popow - Cancer Research UK Dundee Cancer Centre PhD fellowship (C5314/A12975), J.A. Paulo-NIH/NIDDK grant K01 DK098285, M.H. Tatham - supported by Cancer Research UK program grant to R. Hay (C434/A13067), A. Rojas-Fernandez-FONDECYT 11150532 and PAI79150075, N. Loyer and J. Januschke-Sir Henry Dale fellowship to J. Januschke (Wellcome/Royal Society: 100031Z/12/Z), M. Volk - Wellcome Trust PhD fellowship (WT 203962/Z/16/A), Kevin M. Haigis - NIH/NCI grant U01CA199252, and I.P. Newton and I. Näthke - Cancer Research UK program grant to I. Näthke (C430/A11243). We would like to acknowledge the Nikon Imaging Center at Harvard Medical School (Boston, MA) and the Dundee Tissue Imaging Facility at the School of Life Sciences, University of Dundee (Scotland, United Kingdom; supported by Wellcome grant WT101468) for providing help and equipment for microscopy imaging of cells and live *Drosophila* samples, respectively. Stocks from the Bloomington Drosophila Stock Center, which is supported by NIH grant P40OD018537, were used in this study. We would like to thank C. MacKintosh, G. Murugesan, R. Hay, E. Jaffrey, T. Kurz, and M. Keuss (all University of Dundee, Scotland, United Kingdom) for sharing advice and reagents. For their help in the realization of TMT MS experiments, we would like to thank S. Gygi and the Taplin Mass Spectrometry Facility at Harvard Medical School (Boston, MA).

References

1. Miyoshi Y, Nagase H, Ando H, Horii A, Ichii S, Nakatsuru S, et al. Somatic mutations of the APC gene in colorectal tumors: mutation cluster region in the *APC* gene. Hum Mol Genet 1992;1:229–33. [PubMed: 1338904]
2. Powell SM, Zilz N, Beazer-Barclay Y, Bryan TM, Hamilton SR, Thibodeau SN, et al. APC mutations occur early during colorectal tumorigenesis. Nature 1992;359:235–7. [PubMed: 1528264]
3. Leoz ML, Carballal S, Moreira L, Ocaña T, Balaguer F. The genetic basis of familial adenomatous polyposis and its implications for clinical practice and risk management. Appl Clin Genet 2015;8:95–107. [PubMed: 25931827]
4. Stamos JL, Weis WI. The β-catenin destruction complex. Cold Spring Harb Perspect Biol 2013;5:a007898. [PubMed: 23169527]
5. Polakis P Wnt signaling and cancer. Genes Dev 2000;14:1837–51. [PubMed: 10921899]
6. Cheung AF, Carter AM, Kostova KK, Woodruff JF, Crowley D, Bronson RT, et al. Complete deletion of Apc results in severe polyposis in mice. Oncogene 2010;29:1857–64. [PubMed: 20010873]
7. Nelson S, Näthke IS. Interactions and functions of the Adenomatous polyposis coli (APC) protein at a glance. J Cell Sci 2013;126:873–7. [PubMed: 23589686]
8. Breitman M, Zilberberg A, Caspi M, Rosin-Arbesfeld R. The armadillo repeat domain of the APC tumor suppressor protein interacts with Striatin family members. Biochim Biophys Acta 2008;1783:1792–802. [PubMed: 18502210]
9. Bandyopadhyay S, Chiang C, Srivastava J, Gersten M, White S, Bell R, et al. A human MAP kinase interactome. Nat Methods 2010;7:801–5. [PubMed: 20936779]
10. Hein MY, Hubner NC, Poser I, Cox J, Nagaraj N, Toyoda Y, et al. A human interactome in three quantitative dimensions organized by stoichiometries and abundances. Cell 2015;163:712–23. [PubMed: 26496610]
11. Song J, Hao Y, Du Z, Wang Z, Ewing RM. Identifying novel protein complexes in cancer cells using epitope-tagging of endogenous human genes and affinity-purification mass spectrometry. J Proteome Res 2012;11:5630–41. [PubMed: 23106643]
12. Harris BZ, Lim WA. Mechanism and role of PDZ domains in signaling complex assembly. J Cell Sci 2001;114:3219–31. [PubMed: 11591811]
13. Joslyn G, Richardson DS, White R, Alber T. Dimer formation by an N-terminal coiled coil in the APC protein. Proc Natl Acad Sci U S A 1993;90:11109–13. [PubMed: 8248216]
14. Kim NG, Xu C, Gumbiner BM. Identification of targets of the Wnt pathway destruction complex in addition to beta-catenin. Proc Natl Acad Sci U S A 2009;106:5165–70. [PubMed: 19289839]
15. Coyaud E, Mis M, Laurent EMN, Dunham WH, Couzens AL, Robitaille M, et al. BioID-based identification of Skp Cullin F-box (SCF)β-TrCP1/2 E3 ligase substrates. Mol Cell Proteomics 2015;14:1781–95. [PubMed: 25900982]
16. Rojas-Fernandez A, Herhaus L, Macartney T, Lachaud C, Hay RT, Sapkota GP. Rapid generation of endogenously driven transcriptional reporters in cells through CRISPR/Cas9. Sci Rep 2015;5:9811. [PubMed: 25922883]
17. Aberle H, Bauer A, Stappert J, Kispert A, Kemler R. Beta-catenin is a target for the ubiquitin-proteasome pathway. EMBO J 1997;16:3797–804. [PubMed: 9233789]
18. Midgley CA, White S, Howitt R, Save V, Dunlop MG, Hall PA, et al. APC expression in normal human tissues. J Pathol 1997;181:426–33. [PubMed: 9196441]
19. Hinck L, Näthke IS, Papkoff J, Nelson WJ. Dynamics of cadherin/catenin complex formation: novel protein interactions and pathways of complex assembly. J Cell Biol 1994;125:1327–40. [PubMed: 8207061]
20. Schindelin J, Arganda-Carreras I, Frise E, Kaynig V, Longair M, Pietzsch T, et al. Fiji: an open-source platform for biological-image analysis. Nat Methods 2012;9:676–82. [PubMed: 22743772]
21. Pfaffl MW. A new mathematical model for relative quantification in real-time RT-PCR. Nucleic Acids Res 2001;29:e45. [PubMed: 11328886]

22. Shevchenko A, Tomas H, Havlis J, Olsen JV, Mann M. In-gel digestion for mass spectrometric characterization of proteins and proteomes. Nat Protoc 2006;1:2856–60. [PubMed: 17406544]
23. Paulo JA, O'Connell JD, Everley RA, O'Brian J, Gygi MA, Gygi SP. Quantitative mass spectrometry-based multiplexing compares the abundance of 5000 S. cerevisiae proteins across 10 carbon sources. J Proteomics 2016;148:85–93. [PubMed: 27432472]
24. Paulo JP, O'Connell JD, Gygi SP. A Triple Knockout (TKO) proteomics standard for diagnosing ion interference in isobaric labeling experiments. J Am Soc Mass Spectrom 2016;27:1620–5. [PubMed: 27400695]
25. Cox J, Mann M. MaxQuant enables high peptide identification rates, individualized p.p.b.-range mass accuracies and proteome-wide protein quantification. Nat Biotechnol 2008;26:1367–72. [PubMed: 19029910]
26. Tyanova S, Temu T, Sinitcyn P, Carlson A, Hein MY, Geiger T, et al. The Perseus computational platform for comprehensive analysis of (prote) omics data. Nat Methods 2016;13:731–40. [PubMed: 27348712]
27. Shannon P, Markiel A, Ozier O, Baliga NS, Wang JT, Ramage D, et al. Cytoscape: a software environment for integrated models of biomolecular interaction networks. Genome Res 2003;13:2498–504. [PubMed: 14597658]
28. Orchard S, Ammari M, Aranda B, Breuza L, Briganti L, Broackes-Carter F, et al. The MIntAct project-IntAct as a common curation platform for 11 molecular interaction databases. Nucleic Acids Res 2014;42:D358–63. [PubMed: 24234451]
29. Stark C, Breitkreutz B-J, Reguly T, Boucher L, Breitkreutz A, Tyers M. BioGRID: a general repository for interaction datasets. Nucleic Acids Res 2006;34:D535–9. [PubMed: 16381927]
30. Kim JS, Crooks H, Dracheva T, Nishanian TG, Singh B, Jen J, et al. Oncogenic β-catenin is required for bone morphogenetic protein 4 expression in human cancer cells. Cancer Res 2002;62:2744–8. [PubMed: 12019147]
31. Preitner N, Quan J, Nowakowski DW, Hancock ML, Shi J, Tcherkezian J, et al. APC is an RNA-binding protein, and its interactome provides a link to neural development and microtubule assembly. Cell 2014;158:368–82. [PubMed: 25036633]
32. Wiśniewski JR, Duś-Szachniewicz K, Ostasiewicz P, Zióøkowski P, Rakus D, Mann M. Absolute proteome analysis of colorectal mucosa, adenoma, and cancer reveals drastic changes in fatty acid metabolism and plasma membrane transporters. J Proteome Res 2015;14:4005–18. [PubMed: 26245529]
33. Soucy TA, Smith PG, Milhollen MA, Berger AJ, Gavin JM, Adhikari S, et al. An inhibitor of NEDD8-activating enzyme as a new approach to treat cancer. Nature 2009;458:732–6. [PubMed: 19360080]
34. Hu Y, Leo C, Yu S, Huang BCB, Wang H, Shen M, et al. Identification and functional characterization of a novel human misshapen/Nck interacting kinase-related kinase, hMINK beta. J Biol Chem 2004;279:54387–97. [PubMed: 15469942]
35. Caruana G Genetic studies define MAGUK proteins as regulators of epithelial cell polarity. Int J Dev Biol 2002;46:511–8. [PubMed: 12141438]
36. Mimori-Kiyosue Y, Matsui C, Sasaki H, Tsukita S. Adenomatous polyposis coli (APC) protein regulates epithelial cell migration and morphogenesis via PDZ domain-based interactions with plasma membranes. Genes Cells 2007;12:219–33. [PubMed: 17295841]
37. Blundon MA, Schlesinger DR, Parthasarathy A, Smith SL, Kolev HM, Vinson DA, et al. Proteomic analysis reveals APC-dependent posttranslational modifications and identifies novel regulator of β-catenin. Development 2016;143:2629–40. [PubMed: 27287809]
38. Mi L, Zhu F, Yang X, Lu J, Zheng Y, Zhao Q, et al. The metastatic suppressor NDRG1 inhibits EMT, migration and invasion through interaction and promotion of caveolin-1 ubiquitylation in human colorectal cancer cells. Oncogene 2017;36:4323–35. [PubMed: 28346422]
39. Daulat AM, Luu O, Sing A, Zhang L, Wrana JL, McNeill H, et al. Mink1 regulates β-catenin-independent Wnt signaling via Prickle phosphorylation. Mol Cell Biol 2012;32:173–85. [PubMed: 22037766]
40. Mikrykov A, Moss T. Agonistic and antagonistic roles for TNIK and MINK in non-canonical and canonical Wnt signalling. PLoS One 2012;7:e43330. [PubMed: 22984420]

41. Hyodo T, Ito S, Hasegawa H, Asano E, Maeda M, Urano T, et al. Misshapen-like kinase 1 (MINK1) is a novel component of striatin-interacting phosphatase and kinase (STRIPAK) and is required for the completion of cytokinesis. J Biol Chem 2012;287:25019–29. [PubMed: 22665485]
42. Wong MH, Hermiston ML, Syder AJ, Gordon JI. Forced expression of the tumor suppressor adenomatosis polyposis coli protein induces disordered cell migration in the intestinal epithelium. Proc Natl Acad Sci U S A 1996;93:9588–93. [PubMed: 8790374]
43. Mahmoud NN, Boolbol SK, Bilinski RT, Martucci C, Chadburn A, Bertagnolli MM. Apc gene mutation is associated with a dominant-negative effect upon intestinal cell migration. Cancer Res 1997;57:5045–50. [PubMed: 9371501]
44. Caldwell CM, Green RA, Kaplan KB. APC mutations lead to cytokinetic failures in vitro and tetraploid genotypes in Min mice. J Cell Biol 2007;178:1109–20. [PubMed: 17893240]
45. Yamada T, Masuda M. Emergence of TNIK inhibitors in cancer therapeutics. Cancer Sci 2017;108:818–23. [PubMed: 28208209]
46. Sansom OJ, Reed KR, Hayes AJ, Ireland H, Brinkmann H, Newton IP, et al. Loss of Apc in vivo immediately perturbs Wnt signaling, differentiation, and migration. Genes Dev 2004;18:1385–90. [PubMed: 15198980]
47. Paricio N, Feiguin F, Boutros M, Eaton S, Mlodzik M. The Drosophila STE20-like kinase misshapen is required downstream of the Frizzled receptor in planar polarity signaling. EMBO J 1999;18:4669–78. [PubMed: 10469646]
48. Wallingford JB, Habas R. The developmental biology of Dishevelled: an enigmatic protein governing cell fate and cell polarity. Development 2005;132:4421–36. [PubMed: 16192308]
49. Tusher VG, Tibshirani R, Chu G. Significance analysis of microarrays applied to the ionizing radiation response. Proc Natl Acad Sci U S A 2001;98:5116–21. [PubMed: 11309499]

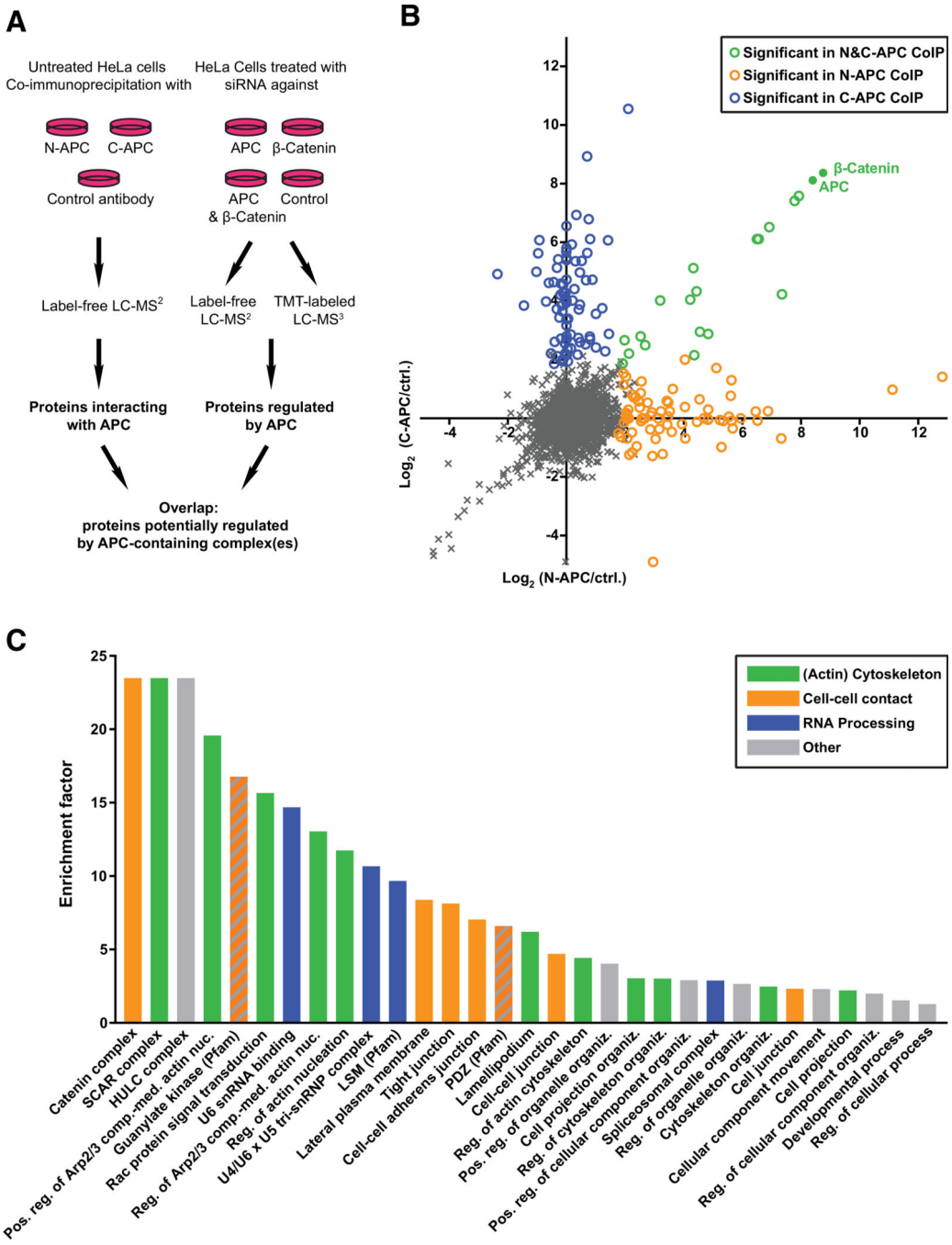

Figure 1.

Identification of APC-interacting and -regulated proteins. **A,** Experimental outline. Proteins in APC-containing complexes and changes in protein expression in response to siRNA-mediated depletion of APC and/or β-catenin were analyzed by label-free and TMT-based mass spectrometry. The overlap between the two datasets constitutes potential targets of alternative APC-containing complexes. **B,** Proteins significantly enriched in C-and/or N-APC co-IPs. Log_2 fold change in mean LFQ intensities between N-APC co-IP versus control IP (*x*-axis) plotted against log_2 fold change in mean LFQ intensities between C-APC

co-IP versus control IP (*y*-axis, $n = 4$ experimental replicates). Significance determined by two-sided *t* test with permutation-based FDR < 0.01 and $s_0 = 2$ used for truncation (49). **C,** GO, Pfam, and KEGG terms significantly enriched in the APC interactome dataset. Enrichment calculated by Fisher exact test, significance determined by Benjamini-Hochberg corrected FDR < 0.02. comp.-med., complex-mediated; nuc., nucleation; organiz., organization; pos., positive; reg., regulation.

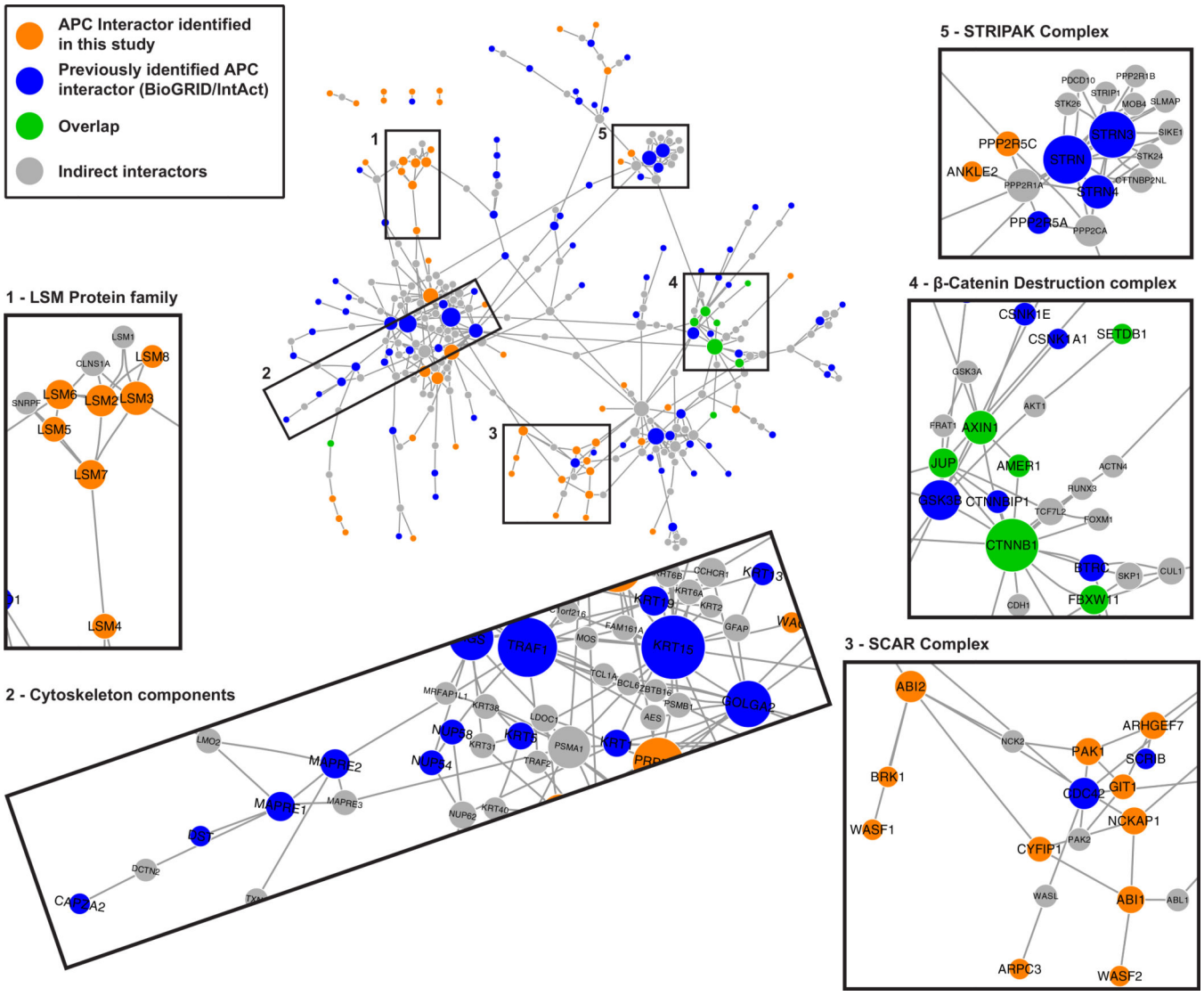

Figure 2.

APC interactome network. Network integrating known (blue), newly identified (orange), and indirect (gray) APC interaction partners. Nodes are labeled with corresponding gene names, and node size correlates with degree of connectivity, that is, number of edges. Components of distinct protein complexes (1, 3–5) and proteins associated with the cytoskeleton (2) cluster together in subnetworks.

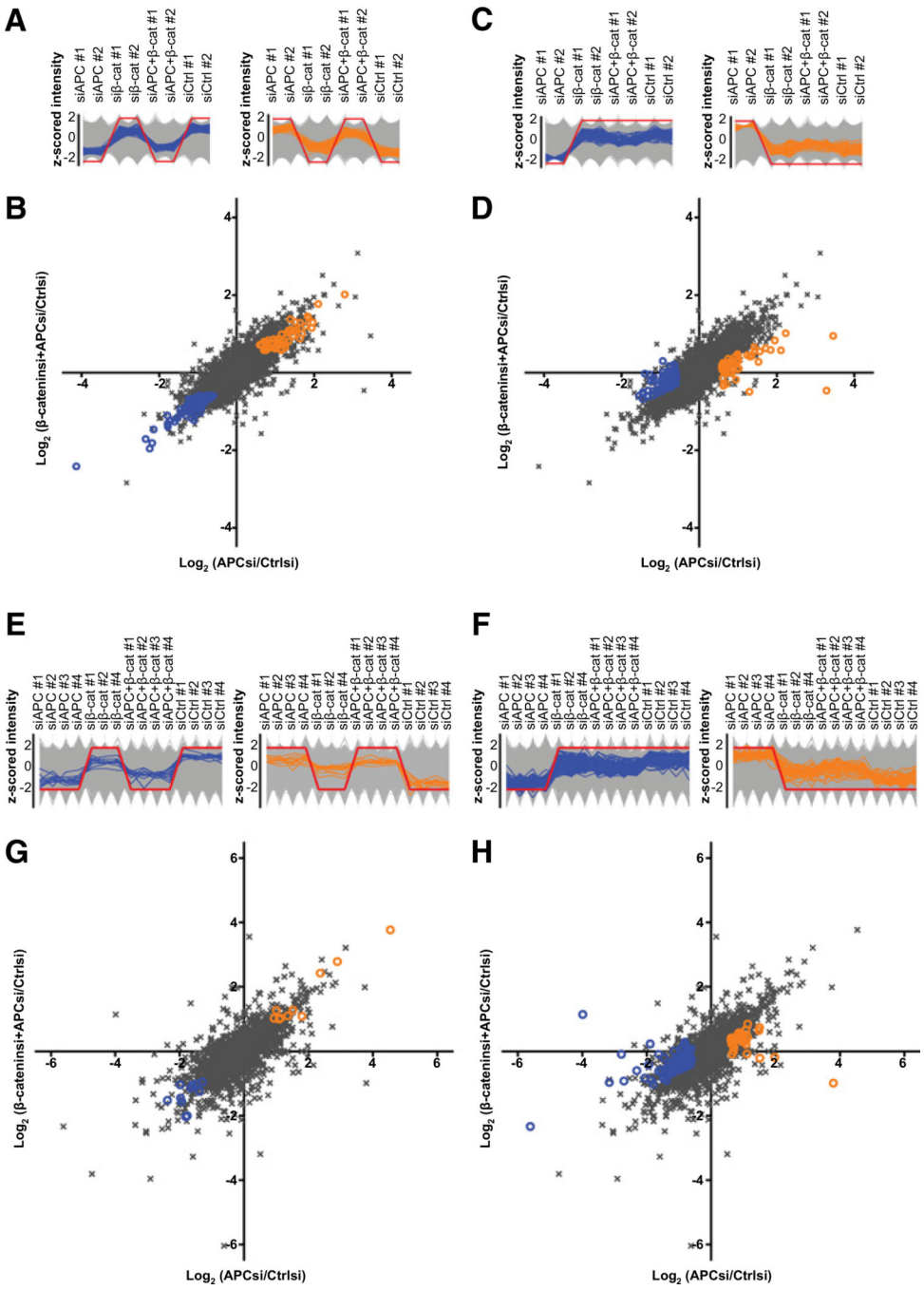

Figure 3.

β-Catenin-dependent and -independent APC targets identified by TMT-label MS (**A-D**) and label-free MS (**E-H**). Profiles of z-scored TMT (**A**) and LFQ (**E**) intensities of all measured proteins across samples. Protein identified as negative and positive β-catenin-independent APC targets are shown in orange and blue, respectively. Red lines show profiles for hypothetical “ideal” targets that increase/decrease in response to APC depletion, but irrespective of a change in β-catenin. Log_2 fold change in mean TMT (**B**) and LFQ (**G**) intensities between APC siRNA and control siRNA-treated samples (*x*-axis) plotted against

the $\log_2$ fold change in mean intensities between β-catenin+APC siRNA and control siRNA-treated samples (*y*-axis). Proteins selected on the basis of their intensity profiles in **A** and **E** are shown in orange and blue, respectively. **C** and **D** same as **A** and **B**, **F** and **H** same as **E** and **G**, but for β-catenin-dependent APC targets.

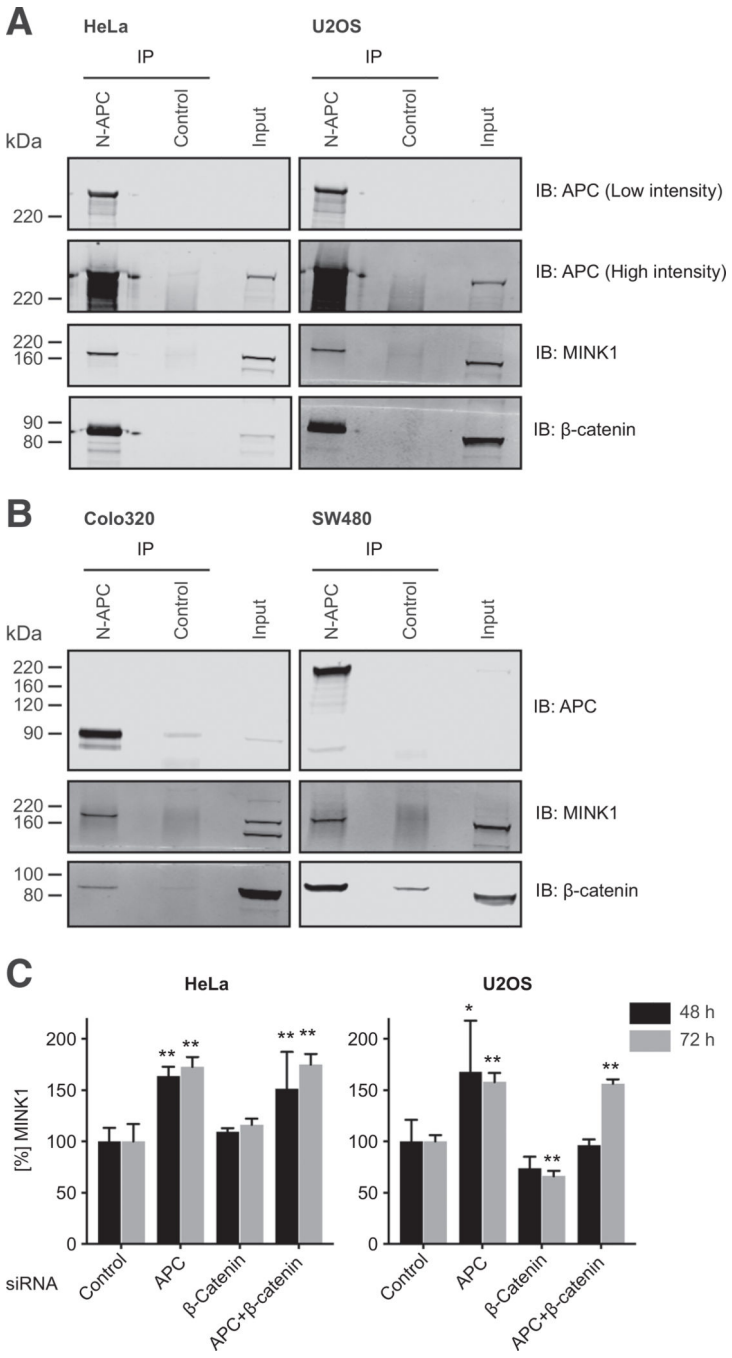

Figure 4.

MINK1 binds to and is negatively regulated by APC. **A**, co-IP of MINK1 with full-length, endogenous APC in HeLa and U2OS cells. **B,** co-IP of MINK1 with C-terminally truncated APC in Colo320 and SW480 colorectal cancer cells; both cell lines lack the WT allele. **C,** Changes in MINK1 proteins levels in response to siRNA-mediated depletion of APC and/or β-catenin measured by WB. Shown are means and SD relative to control samples from four independent transfections. Significance relative to control determined by two-way ANOVA followed by Dunnett multiple comparison test (*, $P < 0.05$; **, $P < 0.01$).

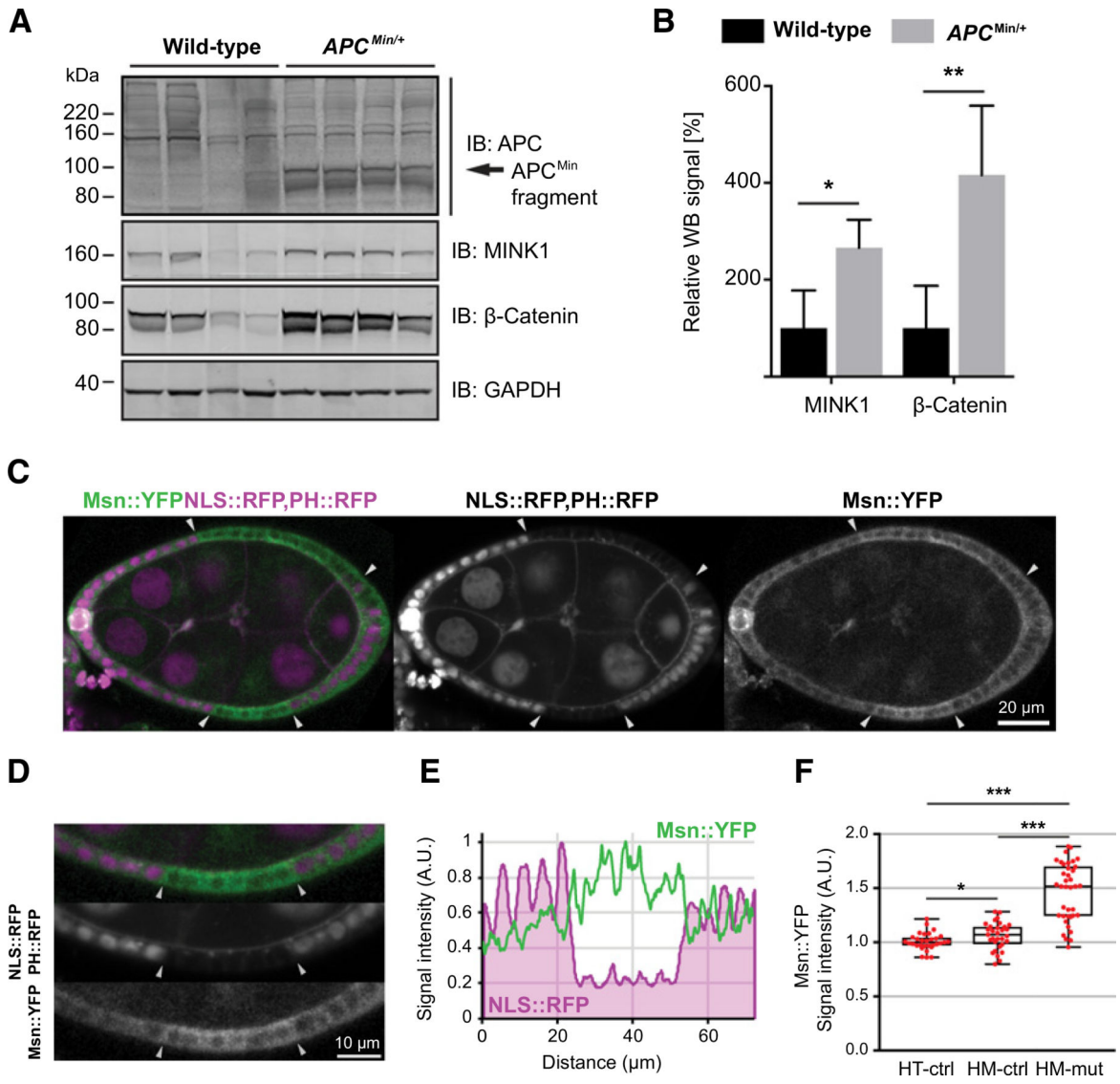

Figure 5.

MINK1/Msn levels increase in response to APC loss *in vivo*. **A,** Expression of MINK1 in small intestinal tissue lysate from WT and *APC*$^{Min/+}$ mice measured by WB; each lane represents lysate obtained from individual mice. The APC^{Min} fragment of approximately 90 kDa was present in mutant mice, but full-length APC (~310 kDa) was not detectable. **B,** Quantification of WB shown in **A**. Shown is the mean WB signal across the 4 mice per genotype relative to the signal in WT mice and normalized to GAPDH. Significance relative to WT samples determined by unpaired, two-tailed *t* test (*, $P < 0.05$; **, $P < 0.01$). **C,** Live stage 8 *Drosophila* egg expressing NLS::RFP and PH::RFP (magenta) under the control of a ubiquitous promoter, and endogenous Msn::YFP (green). Two large *APC1, APC2* double mutant clones within the follicular epithelium are identified by the absence of NLS::RFP and delimited by arrowheads. **D,** Magnification of one *APC1, APC2* double mutant clone displayed in **C**. **E,** Intensity profiles of RFP and Msn::YFP signal along the follicular epithelium. **F,** Msn signal intensity at the interface between *apc1*$^{-}$, *apc2*$^{-}$/*apc1*$^{+}$, *apc2*$^{+}$

heterozygous cells (HT-ctrl, $n = 31$), *apc1*$^{+}$, *apc2*$^{+}$/*apc1*$^{+}$, *apc2*$^{+}$ homozygous control cells (HM-ctrl, $n = 31$), and *apc1*$^{-}$, *apc2*$^{-}$/*apc1*$^{-}$, *apc2*$^{-}$ homozygous mutant cells (HM-mut, $n = 38$), normalized to the signal at heterozygous interfaces. In total, 10 clones from 10 different egg chambers were analyzed. Significance determined by two-tailed Mann-Whitney *U* test (*, $P = 0.0232$; ***, $P < 0.00001$).

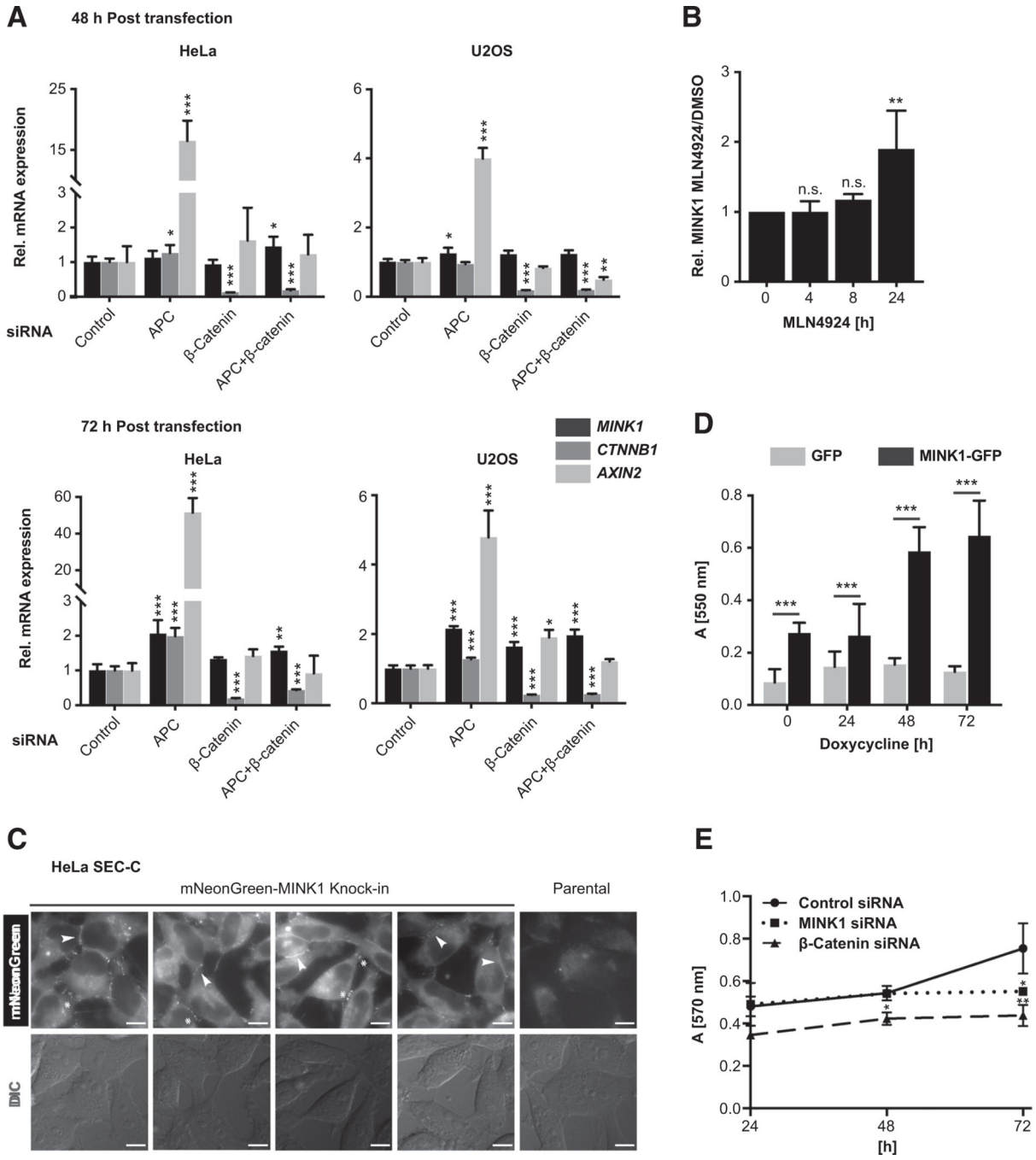

Figure 6.

MINK1 localizes to cell-cell junctions and its overexpression enhances cell adhesion. **A,** mRNA expression of *MINK1, CTNNB1, and AXIN2* measured by qRT-PCR 48 and 72 hours after siRNA transfection. Indicated are mean expression levels relative to *ACTB* expression with SD from four independent transfections. Significance determined by one-way ANOVA followed by Dunnett multiple comparison test (*, $P < 0.05$; **, $P < 0.01$; ***, $P < 0.001$). Note, the same HeLa *AXIN2* mRNA quantification data are also shown in Supplementary Fig. S4D. **B,** MINK1 protein levels in HeLa cells after treatment with

neddylation inhibitor MLN4924 [3 mmol/L] as measured by WB. Shown are relative mean signals normalized to DMSO-treated samples with SD from three independent experiments. Significance determined by one-way ANOVA, **, $P < 0.01$. **C,** Live imaging of HeLa SEC-C cells expressing endogenously mNeonGreen-tagged MINK1. Scale bars, 10 μm. **D,** Adhesion assay with U2OS cells overexpressing MINK1-GFPand GFP, respectively. Adhesion to collagen matrix after 1 hour was quantified by staining of firmly attached cells with Crystal Violet. Indicated is mean absorbance with SD of independent experiments with two different GFP/MINK1-GFP clones and eight technical replicates/condition. Significance determined by two-way ANOVA followed by Sidak multiple comparison test (***, $P < 0.0003$). **E,** MTT proliferation assay in Colo320 cells treated with siRNA against β-catenin or MINK1. Shown is the mean absorbance from triplicate measurements. Significance relative to control determined by one-way ANOVA followed by Dunnett multiple comparison test (*, $P < 0.05$; **, $P < 0.01$). n.s., not significant.

Table 1.

Overlap between β-catenin–independent APC targets identified in this study and proteins misexpressed in colorectal polyps and/or tumors (32)

	Log_2 fold change			q Value			Log_2 fold change (Wiśniewski et al. 2015 - ref 32)	
Protein name (identified by TMT and/or LFQ)	**APC siRNA/ control**	**β-Catenin siRNA/control**	**APC+ β-catenin siRNA/ control**	**APC siRNA/ control**	**β-Catenin siRNA/control**	**APC+ β-catenin siRNA/control**	**Polyps/ normal**	**Tumor/ normal**
60S Ribosomal export protein NMD3 (TMT/LFQ)	2.79/4.54	0.89/2.62	2.02/3.77	<0.001	0.019/0.027	<0.001	0.67	1.46
Peptidyl-prolyl cis-trans isomerase FKBP10 (TMT/LFQ)	1.16/1.13	0.49/0.74	1.00/1.03	0.004/0.04	0.062/0.238	0.003/0.087	0.06	1.95
Melanoma-associated antigen D2 (LFQ)	1.52	1.04	1.29	0.021	0.09	0.047	1.07	2.21
Nucleolar protein 58 (LFQ)	0.93	0.48	1.03	0.059	0.238	0.098	1.5	1.25
6-pyruvoyl tetrahydrobiopterin synthase (TMT)	1.97	0.51	1.29	<0.001	0.057	0.007	1.67	0.66
Glycerophosphocholine phosphodiesterase GPCPD1 (TMT)	1.46	0.41	0.94	0.012	0.083	0.007	1.34	1.19
Hermansky-Pudlak syndrome 5 protein (TMT)	0.74	0.28	0.67	0.002	0.154	0.011	1.14	0.68
Ubiquitin carboxyl-terminal hydrolase 8 (TMT)	1.04	0.44	0.73	0.003	0.069	0.006	0.58	−0.23
Zinc finger protein 622 (TMT)	1.26	−0.19	0.74	0.006	0.283	0.006	0.44	0.80
Ras-related protein Rab-14 (TMT/LFQ)	−1.77/−1.48	−0.08/−0.24	1.39/−1.01	<0.001/0.025	0.568/0.384	<0.001/0.086	−0.55	−0.27
Aldehyde dehydrogenase family 1 member A3 (LFQ)	−1.98	−0.58	1.45	0.009	0.192	0.041	−1.14	−0.69
Dolichol-phosphate mannosyltransferase subunit 1 (TMT)	−1.09	−0.07	0.93	0.004	0.617	0.008	−0.97	0.07
EH domain-containing protein 1 (TMT)	−0.60	−0.20	0.60	0.006	0.229	0.014	−0.95	−0.78
Ferrochelatase, mitochondrial (TMT)	−1.17	−0.04	0.71	0.005	0.751	0.011	−0.33	−1.54
Leucine zipper protein 1 (TMT)	−1.73	−0.20	1.24	<0.001	0.267	0.006	0.85	−0.20
Moesin (TMT)	−1.15	−0.09	0.79	0.003	0.543	0.006	−0.85	−1.06
Nonhistone chromosomal protein HMG-14 (TMT)	−1.28	−0.20	0.85	0.007	0.247	0.006	−0.81	−0.66
Protein NDRG1 (TMT)	−1.55	−0.41	1.18	0.010	0.098	0.004	−0.17	−0.67